IEEE Access
Multidisciplinary : Rapid Review : Open Access Journal

Received 2 August 2024, accepted 19 August 2024, date of publication 23 August 2024, date of current version 4 September 2024.

Digital Object Identifier 10.1109/ACCESS.2024.3449098

RESEARCH ARTICLE

Tuning Performance Parameters of Ge-on-Si Avalanche Photodetector—Part II: Large Bias Operation

YANNING CHEN [1,2], (Member, IEEE), **FANG LIU** [2], **YALI SHAO** [2], **YINGZONG LIANG** [2], **SICHAO DU** [3], (Senior Member, IEEE), AND **WEN-YAN YIN** [3], (Fellow, IEEE)

[1] College of Integrated Circuits, Zhejiang University, Zhejiang 310058, China
[2] Beijing Smart-Chip Microelectronics Technology Company Ltd., Beijing 100192, China
[3] Innovative Institute of Electromagnetic Information and Electronic Engineering, College of Information and Electronic Engineering, Zhejiang University, Hangzhou 310058, China

Corresponding authors: Yanning Chen (chenyanning@sgchip.sgcc.com.cn), Sichao Du (sichaodu@zju.edu.cn), and Wen-Yan Yin (wyyin@zju.edu.cn)

This work was supported in part by the National Natural Science Foundation of China under Grant U23A20350, and in part by the Laboratory Specialized Scientific Research Projects of Beijing Smart-Chip Microelectronics Technology Company Ltd., under Grant SGSCDT00YFQT2400749.

ABSTRACT The carrier multiplication phenomenon involves hot carriers, which gain kinetic energy while accelerating to equilibrium with the established avalanching electric fields, and is typically explained via the local avalanche model. This work presents two vertical Ge-on-Si avalanche photodetectors fabricated in a separate absorption, charge, and multiplication configuration. Uniformity in materials, doping densities, and device dimensions is maintained, except for the multiplication width, which is used as a control parameter to manipulate avalanching fields under identical electric biasing and illumination schemes. Nonlocal carrier multiplication model is implemented during analysis of the extracted current-voltage signatures under small and large reverse biasing arrangements. For such an APD characterized by thinner multiplication region ($W_m = 0.1\ \mu m$), reduced linear and Geiger-mode multiplication regimes are perceived to be at play, outperforming the device having thicker multiplication region in almost all related figures of merit, *e.g.*, responsivity (22.58A/W), photo-to-dark current ratio ($\sim 10^5$), normalized photo-to-dark current ratio ($2.5 \times 10^9 W^{-1}$), specific detectivity (7.45×10^{12}Jones), and noise equivalent power ($\sim 2.42 \times 10^{-15} W/\sqrt{Hz}$). The enhanced performance characteristics are due to excessively strong avalanching fields, reduced thermal charge density, and negligible dead space compared to its counterpart characterized by thicker multiplication width.

INDEX TERMS Avalanche photodetector (APD), Geiger-mode, linear multiplication, vertical Ge-on-Si APD.

I. INTRODUCTION

Avalanche photodetectors (APDs) have long been employed for detecting weak signals, with applications in optical communication, low-light surveillance, photon-limited scientific instruments in astronomy, low-light microscopy, photon counting, and quantum key distribution [1], [2], [3], [4], [5], [6], [7], [8], [9]. Traditionally, group III–V heterostructures, such as InGaAs/InP devices with separate absorption, grading, charge, and multiplication (SAGCM) layers, are used for both linear and Geiger-mode applications in the short wave infrared (SWIR) wavelengths [10], [11], [12], [13].

Ge-on-Si APDs serve as an alternative to III–V heterostructures in terms of materials and applications. They are cost-effective, extend the spectral range relative to silicon, and support industrial-scale production using complementary

The associate editor coordinating the review of this manuscript and approving it for publication was Jiang Wu.

© 2024 The Authors. This work is licensed under a Creative Commons Attribution-NonCommercial-NoDerivatives 4.0 License.
For more information, see https://creativecommons.org/licenses/by-nc-nd/4.0/

metal–oxide–semiconductor (CMOS) manufacturing processes [12]. These APDs can also be effectively used in on-chip optical interconnections within silicon photonic devices, providing hardware support for high-speed optical communications [16], [17]. Several vertical configuration separate absorption, charge, and multiplication (SACM) structures for Ge-on-Si APDs have been reported, focusing on optimizing the dimensions and doping density of different layers to appropriately tailor the electric fields [18], [19], [20].

APDs tailored for linear and Geiger mode operations share structural similarities, often utilizing the same technologies or processes, yet they exhibit distinct differences. Achieving optimal performance in each mode necessitates adjustments in layer thicknesses and doping characteristics, leading to trade-offs between various attributes. In linear-mode operation, a high gain-bandwidth product is beneficial, with the width of the multiplication region (W_m) being inversely proportional to it. Linear-mode APD designs thus necessitate thinner W_m, typically below 1 μm. Contrariwise, the gain-bandwidth product has no direct influence on Geiger-mode operation. Here, thicker W_m is preferred, resulting in lower breakdown fields and reduced tunneling contributions. Therefore, single-photon avalanche detection (SPAD) designs typically configure wider W_m, often exceeding 1 μm [21].

In this work, vertical Ge-on-Si APDs characterized by $W_m = (0.1, 0.5)$ μm are fabricated and subsequently tested for photodetection/carrier multiplication capabilities under 1550 nm wavelength illumination. The devices are tested under similar electrical biasing, and illumination schemes to investigate the dead space region effects over the carrier multiplication capabilities of the devices as nonlocal impact ionization model is considered for elaborating the extracted results. Relatively stronger fields are expected inside Ge-on-Si APD having thin multiplication region (0.1 μm), and vice versa. The obtained results are counter intuitive w.r.t previously discussed threshold $W_m = 1$ μm, distinguishing linear and Geiger mode regimes. We observe that thinning of the multiplication region results in enhanced carrier multiplication capability of the device with additional benefits of reduced punch-through and threshold avalanching voltages directly enabling the investigated APD in low power consumption infrared detection platforms.

The rest of this paper is organized as follows. Section II provides details of the employed fabrication processes, measurement scheme, and a thoughtful discussion of the operational physical mechanisms affecting the results. This is followed by Section III, in which the device's current-voltage ($I - V$) signatures under sweeping bias and unmodulated 1550 nm illumination are presented. It also offers details about various figures of merit, such as responsivity, photo-to-dark current ratio, noise-equivalent power, normalized photo-to-dark current ratio, and specific detectivity. Section IV provides a comparison of the obtained characteristics with various state-of-the-art photodetectors. Finally, we conclude our work in Section V.

II. DEVICE FABRICATION AND WORKING PRINCIPLE

Carrier multiplication events are usually described through "local" ionization coefficients, α for electrons and β for holes. These are equal to the inverse of the mean distance a carrier travels before ionizing. They increase rapidly with the electric field, since only at high fields can carriers attain adequate energy to impact ionize and still maintain the conservation of energy and crystal momentum. The term 'local' implies that ionization coefficients α and β are solely dependent on the local electric field. However, this assumption is never completely correct. Injected carriers acquiring thermal energies, have to travel a certain distance down the field before their distribution in energy heats, and the relevant ionization coefficient attains equilibrium with the field. Within this so-called 'dead space,' carrier multiplication is not plausible. Previously, fabrication technologies were not sophisticated enough to form very thin multiplication regions, consequently requiring very large applied bias ($\sim$100 V) to reduce the ionization path lengths and achieve a multiplication factor of $\sim$100 [22]. Under such large biasing schemes, the dead space, usually of the order of a few tenths of a micron, could then be ignored, and the local approximation was fairly logical. However, a non-local carrier multiplication model becomes more relevant at small applied bias, where a carrier has to inevitably accelerate over relatively longer distances before becoming a "hot" carrier.

We have prepared devices in the SACM PIN configuration [15] characterized with $W_m's$ of 0.1 μm and 0.5 μm, as shown in tabular form in Fig. 1a. This is to investigate the electric field intensities effects over multiplication quantification while keeping all fabrication, illumination, and electrical biasing conditions similar. Under similar biasing conditions, with the increase of W_m, inevitable dead space is incorporated, directly manipulating the multiplication capability of the device. Initially, a 0.1 μm thick N^{++} silicon contact layer ($1.0 \times 10^{20} cm^{-3}$) is grown on a 100 μm thick high-resistivity silicon substrate. Next, the silicon-based multiplication layer ($1.0 \times 10^{15} cm^{-3}$) is sequentially grown. Following this, a 0.1 μm thick p-doped silicon film ($1.0 \times 10^{17} cm^{-3}$) serving as the charge layer is deposited. This is followed by the deposition of a 1 μm thick Ge absorber layer ($1.0 \times 10^{15} cm^{-3}$), which can photoionize under 1550 nm illumination. Finally, a 0.1 μm thick P^{++} Ge contact layer ($1.0 \times 10^{20} cm^{-3}$) is grown on top of the absorber layer.

The ready to test packaged Ge-on-Si APD is shown in Fig.1b (left side). Whereas, the related electrical circuitry for measuring current (I) conducting through Ge-on-Si APD is represented on the right-side of Fig. 1(b). Various colors merely illustrate different constituent layers. We have implemented a Programmable Keithley 4200A-SCS Waveform Analyzer which provides the AC input signal V, and records the corresponding currents conducting through the device.

The voltage is applied in sweeping fashion ranging between $(-2, 1)\ V$ and $(-50, 1)\ V$.

On the left side of Fig.1c, it is emphasized that photo-generated carriers in the Ge absorber under normal incidence of 1550 nm unmodulated illumination experience high carrier multiplication, once they transport into 0.1 μm thick multiplication region in a rather "cold" manner. This is realized via very strong electric field established inside multiplication region. At relatively small bias, the charge layer is incapable of sufficiently accelerating the carriers before entering the multiplication region. But, presence of very large electric field results in negligible dead space length (10 nm). The right side of Fig.1c depicts that via changing the W_m to 0.5 μm, the electric field strength is compromised inside the multiplication region. Although the electric field is still higher than avalanching threshold ($\sim 1.5 \times 10^5$V/cm) [23]. The carrier has to accelerate prior to gaining sufficient energy to cause impact ionization. An inevitable dead space ($\sim 100 - 200\ nm$) , is incorporated into the device operation. The dead space inside the widened multiplication region (0.5 μm) is a zone, where photogenerated carriers accelerate without causing ionization events.

(a)

Materials	Doping Densities	Thicknesses
P^{++} Ge Contact	1.0×10^{20} cm^{-3}	0.1 μm
Ge Absorber	1.0×10^{15} cm^{-3}	1 μm
P-Si Charge Layer	1.0×10^{17} cm^{-3}	0.1 μm
Multiplication Layer	1.0×10^{15} cm^{-3}	0.1 μm, 0.5 μm
N^{++} Si Contact	1.0×10^{20} cm^{-3}	0.1 μm
Silicon Substrate	High Resistance	100 μm

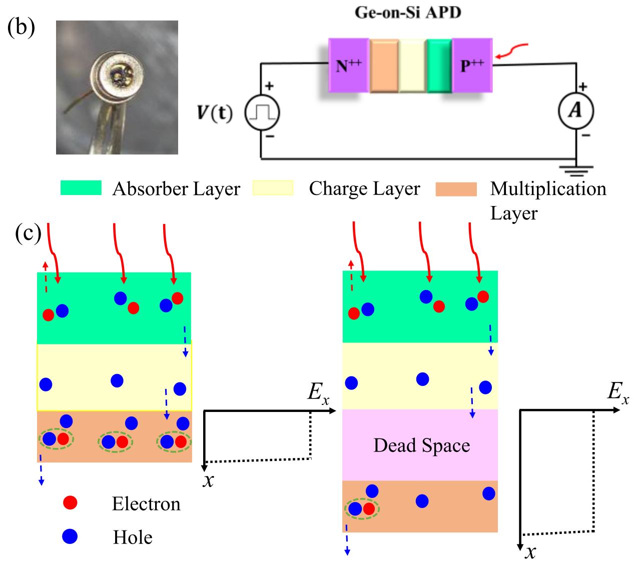

FIGURE 1. For the selectively and epitaxially grown separate absorption, charge, and multiplication configuration Ge-on-Si APD, (a) Various constituent materials, their thicknesses, doping types, and densities are shown in tabular form. (b) The actual vertical Ge-on-Si APD in the ready-to-test packaged form is shown on the left side, while a pictorial schematic of the electrical biasing scheme is shown on the right side. (c) Left: The photo-generation in the Ge absorber layer under 1550 nm unmodulated illumination shows high carrier multiplication in the 0.1 μm thick multiplication region due excessively strong electric fields. Right: Although, for the device characterized with $W_m = 0.5\ \mu m$, the electric field is still higher than the avalanching threshold, the carriers must accelerate over a longer dead space before gaining sufficient energy to cause impact ionization.

III. RESULTS AND DISCUSSIONS

A. CURRENT VS. VOLTAGE CHARACTERISTICS

We present dark and photo response signatures of the employed Ge-on-Si APDs through I $vs.V$ characteristics as shown in Fig.2. The linearly swept voltage V varies between $(-50, 1)V$, whereas illumination intensity (P) of 1550 nm unmodulated laser is fixed at 40 μW. The presented I curves portray W_m dependent behavior. Open circuit voltage (V_{oc}), usually produced in photodiodes, enabling them for solar cell application is created in both the devices characterized by W_m of 0.1 μm, and 0.5 μm. Conventionally, when reverse biasing across an APD is increased, the dark current which is usually of the order of $(10-100)\ nA$ suddenly increases, once the punch-through voltage is reached (beyond this voltage APD functions in the linear multiplication mode, *i.e.*, carrier multiplication is linearly related to the input power density, and applied bias). The further increase of the reverse biasing beyond the avalanche threshold voltage, sets the device in the Geiger-mode operation where single or few photo ionized carriers result in a significant measureable and sustainable current level.

The measurements shown in Fig.2, exhibit that for the Ge-on-Si APD characterized by $W_m = 0.1\ \mu m$, punch-through voltage is reduced to $\sim (-0.15, -0.25)\ V$, while avalanche threshold voltage is also indefinitely reduced. The same device also functions even better under dark condition, resulting from reduced thermal charge density. Subsequently, thermal carriers are not significantly amplified over all of the employed reverse bias range. These I signatures, clearly indicate the initiation of Geiger-mode operation in the voltage range of $-13\ V$ to $-21\ V$, for Ge-on-Si APD characterized by $W_m = 0.5\ \mu m$. This instigates from reduced electric field in multiplication region under similar biasing, as carriers experience enlarged dead space phenomenon. The presented data also highlights a distinguishable photo responses in the forward bias regimes of devices' operation as shown in the inset. With increasing W_m forward biased photo response increases, once sweep bias is larger than 0.6 V, while the reverse trend holds for forward biasing within $(0, 0.6)\ V$ range.

B. RESPONSIVITY

Then, for the employed Ge-on-Si APDs, responsivity (R) which is a metric relating photocurrent (I_{pc}) to the incident illumination P as $R = I_{pc}/P$ is presented in Fig.3. It illustrates a device's capability of converting photo-generated carriers into current flowing through the device that is subsequently readout. The R values larger than one, suggest about carrier multiplication phenomenon at play. The data demonstrated in Fig.3 depicts that for the applied reverse bias $-(50, 0.4)V$ under 40 μW illumination, the APD having W_m of 0.1 μm, is characterized by $R > 1$. This confirms about

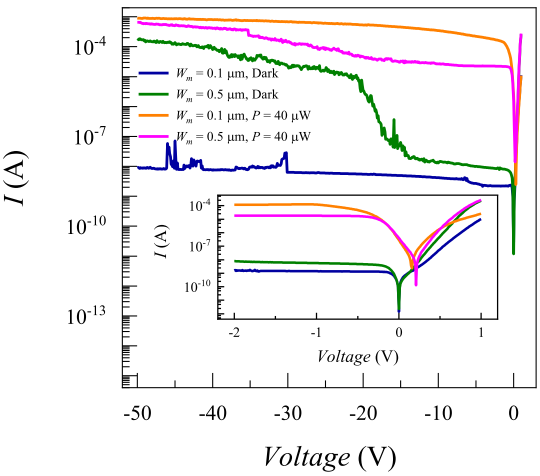

FIGURE 2. **The dark and photocurrent (I) signatures for the employed Ge-on-Si APDs illuminated by an unmodulated intensity of 40 μW, are plotted for W_m values of 0.1 μm and 0.5 μm. The inset corresponds to dark and illuminated measurements under an electrical biasing sweep of $(-2, 1)V$.**

reduced punch-through voltage and indefinitely low voltage Geiger-mode enabled in the device due to multiplication region thinning.

The respective R values at $-50V$ are achieved as 22.58A/W, and 11.88A/W for devices characterized by W_m of 0.1 μm, and 0.5 μm. The comparatively reduced R signature over similar reverse bias range for the APD having 0.5 μm thick multiplication region firstly originate, from the compromised carrier multiplication capability due to the engagement of enlarged dead space, and secondly through the thermal charge multiplication particularly in $-(50, 13)\ V$ bias range. The dark condition multiplication is an absent phenomenon in the thinned device (W_m of 0.1 μm) due to very minuscule thermal charge. The inset focuses on the fact that carrier multiplication ensuring $R > 1$ is enabled in device with W_m of 0.1 μm. While the device characterized by W_m of 0.5 μm has not yet plunged into linear carrier multiplication regime over $(-2, 0)\ V$ sweep range ensuing $R < 1$. Moreover, the R in the forward biased domain is not actual concern of the study.

C. PHOTO-TO-DARK CURRENT RATIO

Subsequently, the capability of the Ge-on-Si APD to act as an illumination controlled switch is shown in Fig.4, via photo-to-dark current ratio ($I_{pc}/I_{dark} = (I - I_{dark})/I_{dark}$) employed as the related figure of merit. Larger I_{pc}/I_{dark} ratios are obtained for the Ge-on-Si APD characterized by W_m of 0.1 μm over all the reverse biased region, approaching $\sim 10^5$ at $V = -50\ V$. It exhibits very similar analogy with previously presented data as punch-through and threshold voltages for linear and Geiger-mode multiplication regimes are reduced due to strong electric field establishments inside thinned multiplication region. Carriers gain impact ionizing momentums very quickly while traversing through negligible dead space region ($\sim 10\ nm$).

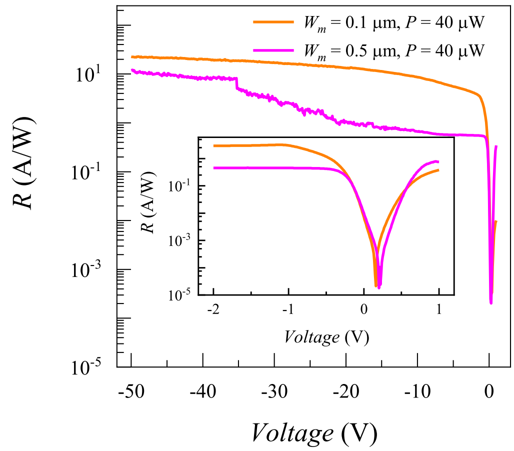

FIGURE 3. **The responsivity (R) signatures for the employed Ge-on-Si APDs illuminated by an unmodulated intensity of 40 μW, are plotted for W_m values of 0.1 μm and 0.5 μm. The inset corresponds to R signatures achieved under an electrical biasing sweep of $(-2, 1)\ V$.**

Under similar biasing scheme for the device having $W_m =$ 0.5 μm, electric field strength is reduced, compromising the carrier multiplication capability of the device as avalanching voltage lies within $-(13, 21)\ V$. Moreover, as density of thermal carriers is enhanced, the subsequent problem of dark current amplification further weakens I_{pc}/I_{dark}. The declining I_{pc}/I_{dark} values within $-(13, 50)V$ is related to thermal charge amplification. Minimum I_{pc}/I_{dark} value of 2.58 is obtained at $V = -50V$. Whereas for the Ge-on-Si APD characterized by W_m of 0.1 μm, I_{pc}/I_{dark} value of $\sim$ 72805 is obtained at $V = -2V$ ensured due to linear multiplication of photo charge and absence of thermal charge amplification as shown in the inset of Fig.4.

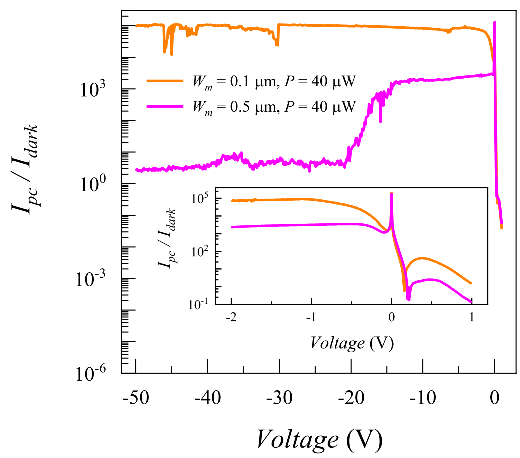

FIGURE 4. **The photo-to-dark current (I_{pc}/I_{dark}) signatures for the employed Ge-on-Si APDs illuminated by an unmodulated intensity of 40 μW, are plotted for W_m values of 0.1 μm and 0.5 μm. The inset corresponds to I_{pc}/I_{dark} signatures achieved under an electrical biasing sweep of $(-2, 1)\ V$.**

D. NORMALIZED PHOTO-TO-DARK CURRENT RATIO

Fig.5 illustrates another figure of merit namely, normalized photo-to-dark-current ratio ($NPDR$) evaluated by normalizing I_{pc}/I_{dark} with reference to input unmodulated illumination intensity P. The $NPDR$ assists comparing R of different photodetectors for a given amount of I_{dark}. Moreover, if the incident wavelength is fixed, one could have a direct comparison of the external quantum efficiency for different detectors for a reference I_{dark}. The $NPDR$ signatures shown in Fig.5 follow the same physical reasoning as stated for previously presented I, R, and I_{pc}/I_{dark} curves. If Fig.4, and Fig.5 are equated, the $NPDR$ signatures for devices having $W_m = (0.1, 0.5)\,\mu m$ and $P = 40\mu W$ are much resembling via scaling of I_{pc}/I_{dark} through P. Similarly, $NDPR$ is also obtained through translation of R via I_{dark}, as shown in the following equation,

$$NPDR = \frac{I_{pc}/I_{dark}}{P} = \frac{I_{pc}/P}{I_{dark}} = \frac{R}{I_{dark}}.$$

The corresponding $NPDR$ values achieved at $V = -50V$ for devices having $W_m's$ of $(0.1, 0.5)\,\mu m$ are $(2.5\times10^9, 6.45\times10^4)\mathrm{W}^{-1}$. The inset presents $NPDR$ signatures extracted over sweep range of $(-2, 1)\,V$. The related maxima achieved at $V = -2V$ are $(1.82\times10^9, 5.77\times10^7)\mathrm{W}^{-1}$. Conclusively, low $NPDR$ values even achieved at the large reverse bias voltages originate due to higher thermal charge density produced in thick space charge region, reduced photo carrier multiplication, enlarged dead space and higher probability of thermal charge multiplication.

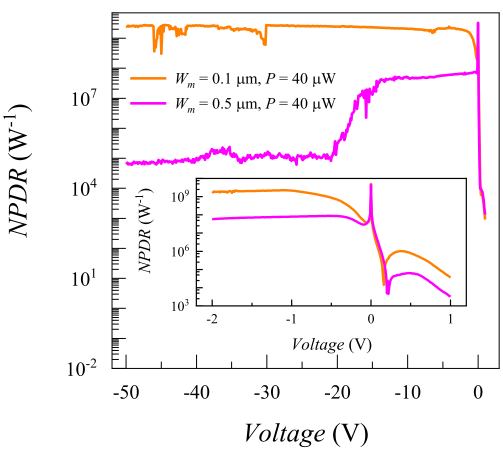

FIGURE 5. The normalized photo-to-dark current (*NPDR*) signatures for the employed Ge-on-Si APDs illuminated by an unmodulated intensity of 40 μW, are plotted for W_m values of 0.1 μm and 0.5 μm. The inset corresponds to *NPDR* signatures achieved under an electrical biasing sweep of $(-2, 1)\,V$.

E. NOISE-EQUIVALENT POWER

Furthermore, we plot noise-equivalent-power (NEP), which is a metric to evaluate optical power for SNR of 1, while a good photodetector is characterized by a low NEP. From data demonstrated in Fig.6, we accomplish that Ge-on-Si APD having W_m of 0.1 μm, perform noticeably well at 40 μW illumination resulting in lowest NEP value at $V = -50V$ approaching $\sim 2.42\times10^{-15}\mathrm{W}/\sqrt{\mathrm{Hz}}$, thanks to enhanced carrier multiplication capability of the device under illumination and almost negligible multiplication of the thermal carriers resulting from the thinning of multiplication region.

Whereas, the Ge-on-Si APD characterized by $W_m = 0.5\,\mu m$, perform reasonably well up to $-13V$ in the reverse biased region, and experiences performance deterioration once thermal carriers are also amplified within $-(50, 13)\,V$ requiring large illumination to deal with thermal carriers density boost. A large NEP value of $6.46\times10^{-13}\mathrm{W}/\sqrt{\mathrm{Hz}}$ obtained at $V = -50V$ for device having W_m of 0.5 μm confirms engagement of dead space at play. For the similar device, the slightly improved NEP value ($\sim 10^{-13}\mathrm{W}/\sqrt{\mathrm{Hz}}$) achieved even at the small reverse $V = -2V$ bias voltage as shown in the inset corresponds to low thermal charge density in the absence of Geiger-multiplication mode that is enabled within $-(50, 13)\,V$.

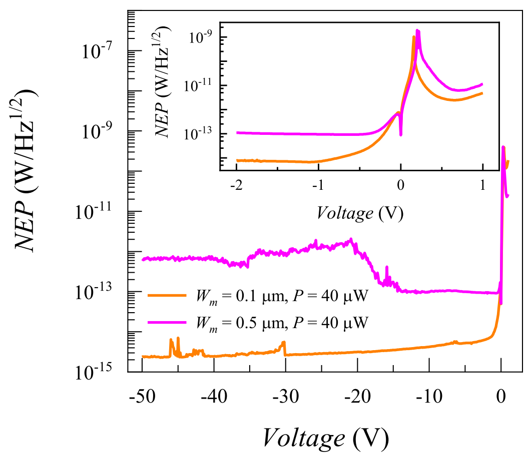

FIGURE 6. The noise-equivalent-power (*NEP*) signatures for the employed Ge-on-Si APDs illuminated by an unmodulated intensity of 40 μW, are plotted for W_m values of 0.1 μm and 0.5 μm. The inset corresponds to *NEP* signatures achieved under an electrical biasing sweep of $(-2, 1)\,V$.

F. SPECIFIC DETECTIVITY

Furthermore, the specific detectivity (D^*) for a certain photodetector having an area (A), and I_{dark} as dark state current, is evaluated employing $D^* = R\sqrt{A}/\sqrt{2eI_{dark}}$ and is demonstrated in Fig.7. It is analogous to the scaling of R through $\sqrt{A}/\sqrt{2eI_{dark}}$ or translation of $NPDR$ via $\sqrt{AI_{dark}/2e}$. Specific detectivity helps in comparing photo detection related figures of merit of devices categorized by different active areas, under similar I_{dark}.

The Ge-on-Si APD having W_m of 0.1 μm, offers higher D^* values throughout the reverse biased regime approaching a maximum of 7.45×10^{12}Jones at $V = -50\,V$, owing to better impact ionization plausibility of photo carriers, due to thinning of multiplication region which boosts electric field way beyond the Geiger-mode avalanche threshold, and reduces the thermal charge multiplication contribution due to minuscule thermal charge generation. Then, for the device having W_m of 0.5 μm, rather compromised D^* values in reverse biased regime approaching a minimum of 2.7×10^{10}Jones at $V = -50V$, result from dead space incorporation at one

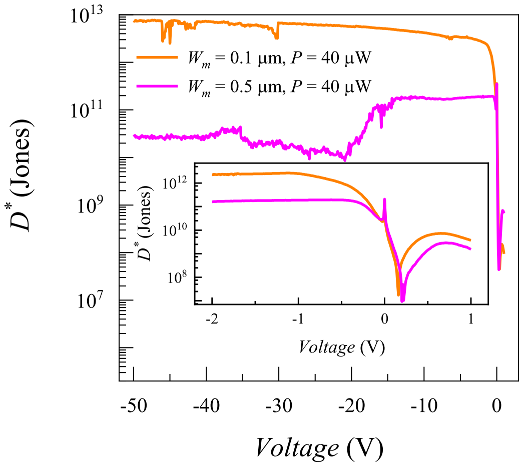

FIGURE 7. The specific detectivity (D^*) signatures for the employed Ge-on-Si APDs illuminated by an unmodulated intensity of 40 μW, are plotted for W_m values of 0.1 μm and 0.5 μm. The inset corresponds to D^* signatures achieved under an electrical biasing sweep of $(-2, 1)$ V.

TABLE 1. Performance Comparison of The Employed Devices with Various State-of-the-Art APD's.

The "×" Means That The Parameter is Not Provided By The Article.

Device	$\lambda(\mu m)$	$I_{dark}(A)$	R (A/W)	D^* (Jones)	NEP (W/√Hz)	Ref
Commercial Ge PD	1.6	40 μ	×	×	7.5 × 10^{-16}	[12]
Pseudo-Planar Ge-on-Si APD	1.55	5.7 μ	0.41	×	×	[24]
Three-Terminal Ge-on-Si APD	1.55	1 μ	0.08	×	×	[25]
Epitaxial Ge-Si APD	1.31	65 m/cm²	0.54	×	×	[26]
Waveguide-Integrated Ge/Si APD	1.55	0.1 n	15.1	×	×	[27]
Negative Differential Ge-on-Si APD	1.55	1.5 μ	0.35	×	×	[28]
Ge-Si SPAD	1.31, 1.55	4 m	×	×	10^{-14}	[29]
Buffer Free Ge/Si SAM APD	1.55	100 μ	12.7	×	×	[30]
Vertical Ge-on-Si APD	1.55	8.9 n 184μ	22.54 11.88	7.45 × 10^{12} 2.7 × 10^{10}	2.42 × 10^{-15} 6.46 × 10^{-13}	This work

hand, and secondly due to the large dark current conducting within $-(50, 13)V$. Whereas, these D^* maxima for devices with $W_m's$ of $(0.1, 0.5)$ μm at $-2V$ reverse bias approach $(2.28 \times 10^{12}, 1.6 \times 10^{11})$Jones as shown in the inset.

IV. COMPARISON WITH THE STATE-OF-THE-ART APDS

Finally, TABLE 1 provides a detailed comparison of the measured or extracted parameters from our vertical SACM configuration Ge-on-Si APDs, categorized by $W_m's$ of 0.1 μm and 0.5 μm. The avalanche-based devices used for comparison come from diverse configurations, fabrication methods, and application areas.

The cost-effective manufacturing of the presented APDs makes them suitable for integration into silicon photonic platforms. This design is also easily adaptable for free-space next-generation sensing, LiDAR, adaptive optics, and imaging applications. The low dark current and enhanced responsivity meet the demands of autonomous driving and other applications requiring weak light detection. The distinct carrier generation characteristics of light and leakage current imply that carriers generated at different positions should be considered separately. We also plan to analyze the examined devices using the innovative history-dependent avalanche model, which could explain the usual abnormal increase in the excess noise factor observed in APDs [31].

V. CONCLUSION

Two vertical Ge-on-Si APDs are fabricated in SACM PIN configuration by assuring uniformity of employed fabrication processes in context of materials, doping densities, and device dimensions. The multiplication width is implemented as a control parameter for manipulating avalanching fields under identical electric biasing and illumination schemes. Nonlocal carrier multiplication model is implemented during analysis of the extracted current-voltage signatures. For the device characterized by $W_m = 0.5$ μm, carriers have to accelerate over an inevitable larger dead space before acquiring sufficient momentum to initiate impact ionization, thus compromising it's multiplication capability. Such device also suffers from larger thermal charge density which will further deteriorate overall performance once these thermal carriers are amplified under both linear, and Geiger mode regimes. The respective compromised figures of merit *e.g.,* R, I_{ph}/I_{dark}, $NPDR$, NEP, and D^* obtained from APDs characterized by thicker multiplication region are 11.88A/W, 2.58, $6.45 \times 10^4 W^{-1}$, $6.46 \times 10^{-13} W/\sqrt{Hz}$, and 2.7×10^{10}Jones. Both of the APDs find solar cell application, owing to the illumination induced open circuit voltage, and low operational power requiring environments *e.g.,* LiDAR.

REFERENCES

[1] C. Bruschini, H. Homulle, I. M. Antolovic, S. Burri, and E. Charbon, "Single-photon avalanche diode imagers in biophotonics: Review and outlook," *Light, Sci. Appl.*, vol. 8, no. 1, p. 87, Sep. 2019, doi: 10.1038/S41377-019-0191-5.

[2] C. Liu, J. Guo, L. Yu, J. Li, M. Zhang, H. Li, Y. Shi, and D. Dai, "Silicon/2D-material photodetectors: From near-infrared to mid-infrared," *Light, Sci. Appl.*, vol. 10, no. 1, pp. 1–26, Jun. 2021, doi: 10.1038/S41377-021-00551-4.

[3] A. B. Kravchenko, A. F. Plotnikov, and V. É. Shubin, "A linear array of avalanche MIS photodetectors," *Sov. J. Quantum Electron.*, vol. 8, no. 11, pp. 1399–1400, Nov. 1978, doi: 10.1070/QE1978V008N11ABEH011331.

[4] S. Riazimehr, S. Kataria, J. M. Gonzalez-Medina, S. Wagner, M. Shaygan, S. Suckow, F. G. Ruiz, O. Engström, A. Godoy, and M. C. Lemme, "High responsivity and quantum efficiency of graphene/silicon photodiodes achieved by interdigitating Schottky and gated regions," *ACS Photon.*, vol. 6, no. 1, pp. 107–115, Jan. 2019, doi: 10.1021/ACSPHOTONICS.8B00951.

[5] O. Lopez-Sanchez, D. Lembke, M. Kayci, A. Radenovic, and A. Kis, "Ultrasensitive photodetectors based on monolayer MoS_2," *Nature Nanotechnol.*, vol. 8, no. 7, pp. 497–501, Jul. 2013, doi: 10.1038/NNANO.2013.100.

[6] P. J. Pool, D. J. Burt, and R. T. Bell, "Electron multiplying CCDs," in *Proc. SNIC Symp.*, 2006, pp. 2–7.

[7] D. Renker, ''Geiger-mode avalanche photodiodes, history, properties and problems,'' *Nucl. Instrum. Methods Phys. Res. A, Accel. Spectrom. Detect. Assoc. Equip.*, vol. 567, no. 1, pp. 48–56, Nov. 2006, doi: 10.1016/J.NIMA.2006.05.060.

[8] M. Moszynski, C. Plettner, A. Nassalski, T. Szczesniak, L. Swiderski, A. Syntfeld-Kazuch, W. Czarnacki, G. Pausch, J. Stein, A. Niculae, and H. Soltau, ''A comparative study of silicon drift detectors with photomultipliers, avalanche photodiodes and PIN photodiodes in gamma spectrometry with $LaBr_3$ crystals,'' *IEEE Trans. Nucl. Sci.*, vol. 56, no. 3, pp. 1006–1011, Jun. 2009, doi: 10.1109/TNS.2008.2005110.

[9] A. Rawat, A. Ahamed, C. Bartolo-Perez, A. S. Mayet, L. N. McPhillips, and M. S. Islam, ''Design and fabrication of high-efficiency, low-power, and low-leakage Si-avalanche photodiodes for low-light sensing,'' *ACS Photon.*, vol. 10, no. 5, pp. 1416–1423, May 2023, doi: 10.1021/ACSPHOTONICS.3C00026.

[10] J. C. Campbell, ''Recent advances in avalanche photodiodes,'' *J. Lightw. Technol.*, vol. 34, no. 2, pp. 278–285, Jan. 3, 2016, doi: 10.1109/JLT.2015.2453092.

[11] J. C. Campbell, ''Recent advances in telecommunications avalanche photodiodes,'' *J. Lightw. Technol.*, vol. 25, no. 1, pp. 109–121, May 1, 2007, doi: 10.1109/JLT.2006.888481.

[12] A. Lacaita, P. A. Francese, F. Zappa, and S. Cova, ''Single-photon detection beyond 1 μm: Performance of commercially available germanium photodiodes,'' *Appl. Opt.*, vol. 33, no. 30, p. 6902, 1994.

[13] P. A. Hiskett, G. S. Buller, A. Y. Loudon, J. M. Smith, I. Gontijo, A. C. Walker, P. D. Townsend, and M. J. Robertson, ''Performance and design of InGaAs/InP photodiodes for single-photon counting at 155 μm,'' *Appl. Opt.*, vol. 39, no. 36, p. 6818, 2000, doi: 10.1364/AO.39.006818.

[14] A. Sammak, M. Aminian, L. K. Nanver, and E. Charbon, ''CMOS-compatible PureGaB Ge-on-Si APD pixel arrays,'' *IEEE Trans. Electron Devices*, vol. 63, no. 1, pp. 92–99, Jan. 2016, doi: 10.1109/TED.2015.2457241.

[15] J. Michel, J. Liu, and L. C. Kimerling, ''High-performance Ge-on-Si photodetectors,'' *Nature Photon.*, vol. 4, no. 8, pp. 527–534, Aug. 2010, doi: 10.1038/NPHOTON.2010.157.

[16] H. T. Chen, P. Verheyen, M. Rakowski, P. De Heyn, G. Lepage, J. De Coster, P. Absil, G. Roelkens, and J. Van Campenhout, ''Low-voltage Ge avalanche photodetector for highly sensitive 10Gb/s Si photonics receivers,'' in *Proc. 11th Int. Conf. Group IV Photon. (GFP)*, Aug. 2014, pp. 106–107.

[17] C. Hong, B. Shi, F. Qi, P. Cai, Y. Duan, G. Hou, T. Su, T. Chiu, S. Li, W. Chen, and D. Pan, ''High speed Ge/Si avalanche photodiode with high sensitivity for 50Gbit/s and 100Gbit/s optical access systems,'' in *Proc. Opt. Fiber Commun. Conf. Exhibition (OFC)*, Mar. 2022, pp. 1–3.

[18] X. Zeng, Z. Huang, B. Wang, D. Liang, M. Fiorentino, and R. G. Beausoleil, ''Silicon–germanium avalanche photodiodes with direct control of electric field in charge multiplication region,'' *Optica*, vol. 6, no. 6, p. 772, 2019, doi: 10.1364/OPTICA.6.000772.

[19] Y. Li, X. Liu, X. Li, S. Wang, H. Ye, L. Zhang, Y. Li, S. Sun, B. Chen, Y. Ma, P. Guo, F. Gao, X. Li, G. Lo, and J. Song, ''Surface illuminated interdigitated Ge-on-Si photodetector with high responsivity,'' *Opt. Exp.*, vol. 29, no. 11, p. 16346, 2021, doi: 10.1364/OE.427343.

[20] N. Duan, T.-Y. Liow, A. E.-J. Lim, L. Ding, and G. Q. Lo, ''310 GHz gain-bandwidth product Ge/Si avalanche photodetector for 1550 nm light detection,'' *Opt. Exp.*, vol. 20, no. 10, p. 11031, 2012, doi: 10.1364/OE.20.011031.

[21] D. A. Ramirez, M. M. Hayat, G. Karve, J. C. Campbell, S. N. Torres, B. E. A. Saleh, and M. C. Teich, ''Detection efficiencies and generalized breakdown probabilities for nanosecond-gated near infrared single-photon avalanche photodiodes,'' *IEEE J. Quantum Electron.*, vol. 42, no. 2, pp. 137–145, Feb. 2006, doi: 10.1109/JQE.2005.861627.

[22] G. J. Rees and J. P. R. David, ''Nonlocal impact ionization and avalanche multiplication,'' *J. Phys. D, Appl. Phys.*, vol. 43, no. 24, Jun. 2010, Art. no. 243001, doi: 10.1088/0022-3727/43/24/243001.

[23] S. K. Madan, B. Bhaumik, and J. M. Vasi, ''Experimental observation of avalanche multiplication in charge-coupled devices,'' *IEEE Trans. Electron Devices*, vols. ED-30, no. 6, pp. 694–699, Jun. 1983, doi: 10.1109/T-ED.1983.21191.

[24] F. Fleming, X. Yi, M. M. A. Mirza, X. Jin, J. Kirdoda, D. C. S. Dumas, L. Saalbach, M. Modak, D. A. S. Muir, C. Smith, C. Coughlan, Q. Tian, R. W. Millar, J. P. R. David, D. J. Paul, and G. S. Buller, ''Surface-normal illuminated pseudo-planar Ge-on-Si avalanche photodiodes with high gain and low noise,'' *Opt. Exp.*, vol. 32, no. 11, p. 19449, 2024, doi: 10.1364/OE.521417.

[25] X. Liu, X. Li, Y. Li, Y. Li, Z. Zhi, M. Tao, B. Chen, L. Zhang, P. Guo, G. Lo, X. Li, F. Gao, B. Kang, and J. Song, ''Three-terminal germanium-on-silicon avalanche photodiode with extended p-charge layer for dark current reduction,'' *Photon. Res.*, vol. 10, no. 8, p. 1956, 2022, doi: 10.1364/PRJ.452004.

[26] Y. Kang, M. Zadka, S. Litski, G. Sarid, M. Morse, M. J. Paniccia, Y.-H. Kuo, J. Bowers, A. Beling, H.-D. Liu, D. C. McIntosh, J. Campbell, and A. Pauchard, ''Epitaxially-grown Ge/Si avalanche photodiodes for 1.3 μm light detection,'' *Opt. Exp.*, vol. 16, no. 13, p. 9365, 2008, doi: 10.1364/OE.16.009365.

[27] D. Liu, P. Zhang, B. Tang, W. Wang, and Z. Li, ''High-performance waveguide-integrated Ge/Si avalanche photodetector with lateral multiplication region,'' *Micromachines*, vol. 13, no. 5, p. 649, Apr. 2022, doi: 10.3390/MI13050649.

[28] G. Kim, S. Kim, S. A. Kim, J. H. Oh, and K.-S. Jang, ''NDR-effect vertical-illumination-type Ge-on-Si avalanche photodetector,'' *Opt. Lett.*, vol. 43, no. 22, p. 5583, 2018.

[29] R. E. Warburton, G. Intermite, M. Myronov, P. Allred, D. R. Leadley, K. Gallacher, D. J. Paul, N. J. Pilgrim, L. J. M. Lever, Z. Ikonic, R. W. Kelsall, E. Huante-Cerón, A. P. Knights, and G. S. Buller, ''Ge-on-Si single-photon avalanche diode detectors: Design, modeling, fabrication, and characterization at wavelengths 1310 and 1550 nm,'' *IEEE Trans. Electron Devices*, vols. ED-60, no. 11, pp. 3807–3813, Nov. 2013, doi: 10.1109/TED.2013.2282712.

[30] C.-L. Hsin and C.-H. Chou, ''Buffer-free Ge/Si by rapid melting growth technique for separate absorption and multiplication avalanche photodetectors,'' *IEEE Electron Device Lett.*, vol. 40, no. 6, pp. 945–948, Jun. 2019, doi: 10.1109/LED.2019.2910047.

[31] R. Xie, Q. Li, P. Wang, X. Chen, W. Lu, H. Guo, L. Chen, and W. Hu, ''Spatial description theory of narrow-band single-carrier avalanche photodetectors,'' *Opt. Exp.*, vol. 29, no. 11, p. 16432, 2021, doi: 10.1364/OE.418110.

YANNING CHEN (Member, IEEE) received the B.S. degree in computer science from Capital Normal University, Beijing, China, in 2002, and the M.S. degree in electronic and communication engineering from Beijing University of Posts and Telecommunications, Beijing, in 2018. She is currently pursuing the Ph.D. degree with the IC College, Zhejiang University. She was a Senior Engineer, the Vice Director of Chip Laboratory, and the Executive Director of Beijing Chip Identification Technology Company Ltd. She has long been engaged in industrial chip design and generic technology research. She led the team to study the application environment of power industry chips, formulate relevant technical standards, and establish the quality assurance system of industrial chips.

FANG LIU received the Ph.D. degree from Tianjin University, Tianjin, China, in 2010. Since 2015, she has been joining Beijing Smart-Chip Microelectronics Technology Company Ltd., Beijing, China. Her current research interests include reliability of integrated circuit and semiconductor devices.

YALI SHAO received the B.S. and M.S. degrees in electronic engineering from Zhejiang University, Hangzhou, China, in 2008 and 2011, respectively. She was with Texas Instruments, from 2011 to 2017, and then with Analog Devices, from 2017 to 2021. She was an Expert of analog and analog/mixed-signal design and verification. Her current occupancy is EDA and IP lead with Beijing Smart-Chip Microelectronics Technology Company Ltd., since 2021. Her research interests include process and device simulation of TCAD, IC design automation, and analog and mixed-signal IC design.

YINGZONG LIANG received the M.E. and Ph.D. degrees in systems innovation from The University of Tokyo, Japan, in 2013 and 2017, respectively. He is currently a Senior IC Design Engineer with Beijing Smart-Chip Microelectronics Technology Company Ltd. He was a Postdoctoral Fellow with the Institute of Physics, CAS, from 2019 to 2021. His current research interests include data science, material science, device physics, and IC design combined with AI technologies.

SICHAO DU (Senior Member, IEEE) received the B.S. degree in materials physics from Northwestern Polytechnical University, Xi'an, China, in 2005, the M.Phil. degree in optoelectronics devices and materials from The Australian National University, Australia, in 2009, and the Ph.D. degree in optoelectronics devices and materials from The University of Sydney, Australia, in 2014. In 2016, he joined the School of Information Science and Electronic Engineering, Zhejiang University, as an Overseas Outstanding Postdoctoral Research Fellow. He is currently an Associate Professor and a Principal Investigator with the School of Information and Electrical Engineering, Zhejiang University City College. He established a Laboratory of Single-Photon Detection and Imaging Techniques, Zhejiang Engineering Research Center for Edge Intelligence Technology and Equipment. He has published 40 peer-reviewed journal articles, including *Nature Communications*, *Advanced Materials*, and *Carbon*, with average impact factor 15.7 and 1446 citations from Google Scholar and H-index is 15. Moreover, five articles are ESI highly cited and three articles have been selected as cover image. He has 20 China granted patents and one monography as the Editor-in-Chief. He is a member of MRS and OPTICA. He is mainly engaged in the research of the working principles, device structures and manufacturing processes of advanced photodetectors. The principles of photo-induced charge carriers' generation, transport, recombination, and collection have been symmetrically studied in carbon from nanoscopy, microscopy, mesoscopy to macroscopy. On this basis, his research interests include the design and fabrication of ultra-sensitive optoelectronic devices with the 2D materials and low-dimensional semiconductors, to explore the application potential of non-equilibrated charge carriers for single photon avalanche diodes (SPAD).

WEN-YAN YIN (Fellow, IEEE) received the M.S. degree in electromagnetic fields and microwave techniques from Xidian University, Xi'an, China, in 1989, and the Ph.D. degree in electrical engineering from Xi'an Jiaotong University, Xi'an, in 1994.

From 1993 to 1996, he was an Associate Professor with the Department of Electronic Engineering, Northwestern Polytechnic University (NPU), Xi'an. From 1996 to 1998, he was the AvH Research Fellow of the Department of Electronic Engineering, Duisburg University, Germany. Since December 1998, he has been with the National University of Singapore (NUS), Singapore, as a Research Scientist. From April 2005 to December 2008, he was a Professor with the School of Electronic Information and Electrical Engineering, Shanghai Jiao Tong University (SJTU), Shanghai, China, where he was an Adjunct Ph.D. Candidate Supervisor with the Center for Microwave and RF Technologies, in 2019. Since January 2009, he has been with Zhejiang University (ZJU), Hangzhou, China, as a "Qiu Shi" Distinguished Professor, where he is currently the Director of the Innovative Institute of Electromagnetic Information and Electronic Integration (EIEI), College of Information Science and Electronic Engineering (ISEE). As a leading author, he has published more than 330 international journal articles (more than 200 IEEE papers), including one international book and several book chapters. His main research interests include EMC and EM protection of communication platforms, computational electromagnetics and multiphysics and their applications, nanoelectronics, 3D IC, and advanced packaging.

Dr. Yin received the Science and Technology Progress Award of the First Class from the Local Shanghai Government of China, in 2005 and 2011, respectively, the National Technology Invention Award of the Second Class from Chinese Government, in 2008, the Science and Technology Progress Award of the Second Class of China, in 2012, the Defense Technology Invention Award of the Second Class of China, in 2015, and several best paper awards of the international conferences. He was the General Co-Chair of the 2017 IEEE Electrical Design of Advanced Packaging and Systems Symposium (IEEE EDAPS' 2017), sponsored by the IEEE Electronic Packaging Committee. He was also the Technical Chair of EDAPS' 2006 and 2011, respectively. He is also an Associate Editor of IEEE TRANSACTIONS ON COMPONENTS, PACKAGING AND MANUFACTURING TECHNOLOGY, since 2013. He was also an Associate Editor of IEEE JOURNAL OF MULTISCALE AND MULTIPHYSICS COMPUTATIONAL TECHNIQUES. From 2011 to 2012, he was an IEEE EMC Society Distinguished Lecturer. From January 2013 to December 2016, he was the IEEE EMC Society Chapter Chair. From January 2011 to December 2016, he was an Associate Editor of the *International Journal of Electronic Networks, Devices and Fields*. He was also an Editorial Board Member of *International Journal of RF and Microwave Computer-Aided Engineering*, from January 2012 to December 2014.